Surrogate modelling and heat pump integration of CO_2 capture in multi-vector energy systems

Brieuc Beguin [a] and Grégoire Léonard [b]

[a] University of Liège, Liège, Belgium, brieuc.beguin@uliege.be, CA
[b] University of Liège, Liège, Belgium, g.leonard@uliege.be

Abstract:

Achieving negative emissions through bioenergy with carbon capture and storage (BECCS) requires system-level optimisation to determine optimal design and operation. Recent developments in high-temperature heat pumps enable the partial or full electrification of amine-based CO_2 capture systems. This creates new opportunities for heat integration in multi-vector energy systems. However, their optimisation requires computationally efficient models. This work presents a physics-informed surrogate model of an amine-based CO_2 capture unit integrated into a multi-vector energy system case study. A convergence-assistance algorithm is proposed to generate training data from a high-fidelity Aspen Plus model, achieving a convergence success rate of 96.4%. Physical relationships between input and output variables are considered to define the model structure, and polynomial regression is used to train the surrogate model. Pinch analysis is applied to derive process heat requirements and recoverable waste heat. Then, heat pump integration is investigated using exergy minimisation as a proxy for cost optimisation. The analysis reveals two dominant heat pump integration configurations: a partial integration relying on high-temperature waste heat sources, and a full electrification scenario exploiting low-temperature heat across the entire process. Parameter analysis shows that stripper pressure and lean loading govern the transition between these configurations. This work demonstrates that surrogate models can serve not only for computationally efficient predictions, but also as tools for exploring thermodynamic integration configurations in complex energy systems.

Keywords:

CO_2 capture; High-temperature heat pump; Multi-vector energy systems; Surrogate model.

1. Introduction and motivations

Most emission pathways aimed at meeting climate targets converge towards net-zero emissions. Therefore, so-called “hard-to-abate” emissions must be compensated through carbon dioxide removal (CDR), also known as negative emissions [1]. Bioenergy with carbon capture and storage (BECCS) is currently the most prevalent CDR technology in emission pathways.

Bioenergy is already used in energy systems (e.g. biomass, municipal waste). However, retrofitting these energy systems with carbon capture and storage (CCS) poses a challenge as it introduces a new energy consumer to account for. Therefore, maintaining the energy balance requires careful design and optimal operation. For this purpose, historical demand data can be used to simulate future demand in the system, and an optimisation problem can be formulated. In this context, a CO_2 capture unit model must be developed for integration as a system component.

Most CO_2 capture models are developed using commercial software (e.g. Aspen Plus, UniSim, gPROMS, ProMax), thanks to which accurate results can be obtained for many operating variables. However, their computation time (several seconds per simulation) is incompatible with system-level optimisation. For this reason, surrogate models are an attractive alternative. At the expense of less accurate results, they provide computationally efficient results for a selected set of outputs. This work deals with the development of such a surrogate model.

More specifically, the surrogate model is developed in the context of a multi-vector energy system. Amongst biomass-based energy systems, multi-vector systems offer additional integration opportunities, such as substitution of an energy vector by another (e.g. electrification of the thermal energy supply).

As a case study, we investigate the integration of an amine-based, chemical absorption CO_2 capture unit into the biomass-fired combined heat and power (CHP) plant of the University of Liège, Belgium. The CHP plant

supplies heat to the local district heating network (DHN) and generates electricity with the leftover energy from the biomass boiler. Gas boilers are also available to deal with demand peaks.

The CO_2 capture unit is modelled in Aspen Plus using MEA as the solvent. The flowsheet includes flue gas conditioning, absorption and stripping columns, as well as a CO_2 compression train to prepare the captured CO_2 for injection into the future Belgian CO_2 network, with an assumed pressure of 2000 kPa [2].

The Aspen Plus model is used to generate data points for surrogate model development. The model inputs and outputs are selected based on the intended system integration.

With recent developments in high-temperature heat pumps [3–5], (partial or full) electrification of the studied capture unit can be considered. As a result, depending on energy availability and market conditions, energy supply to the capture system can be dynamically adapted to take advantage of the available energy vectors.

To integrate a high-temperature heat pump into the capture system, the surrogate model must interface coherently with a heat pump model, and its outputs must therefore describe the heating requirements as well as waste heat availability. Both can be mapped together using heat integration methodologies. In this work, we use pinch analysis (see [6] for a detailed description) to derive the process Grand Composite Curve (GCC). With the pinch point acting as a pivot, the GCC represents the potential cold sources (below the pinch point) as well as the hot sinks (above the pinch point). Integrating a heat pump can be formulated as a matching problem between these two regions.

Model inputs are selected to provide sufficient flexibility to the optimiser. For a given load (i.e. amount of CO_2 to be captured), several operating conditions of the capture unit can be optimised to minimise the thermal energy demand of the system (i.e. the reboiler heat duty). However, this energy optimum is not guaranteed to coincide with the cost optimum that a larger system could reach. Depending on market conditions and interactions with other system components, it could be more interesting to operate at off-optimum conditions, or under part-load operation. Stripper pressure is one example of these operating conditions (Figure 1).

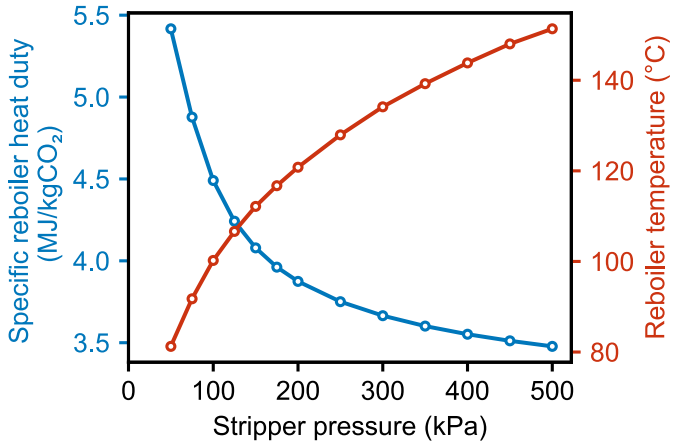

Figure 1. *Stripper pressure is an operating parameter that affects both thermal energy consumption and the temperature at which heat must be supplied. If heat is supplied by heat pumping instead of fuel combustion, the supply temperature becomes a critical parameter, and stripper pressure must be optimised.*

After identifying the relevant operating parameters (Section 2.1), we generate various sample conditions (Section 2.2) at which the high-fidelity Aspen Plus model is evaluated (Section 2.3). The resulting input-output data points are used to train (Section 2.4) and validate (Section 2.5) the surrogate model. Heat pump integration is then investigated (Section 3).

2. Surrogate model development

2.1. Definition of model variables

Four operating parameters are selected as model inputs: flue gas flow rate (enabling part-load operation), lean loading (off-optimum operation), stripper pressure (trade-off between heat demand and supply temperature), and capture rate (also part-load operation). These inputs provide sufficient flexibility to the optimiser. In particular, lean loading, which characterises the solvent CO_2 content, strongly influences the reboiler heat duty and exhibits an optimal value [7,8]. However, the optimum shifts with other operating conditions. It is therefore retained as an independent input variable.

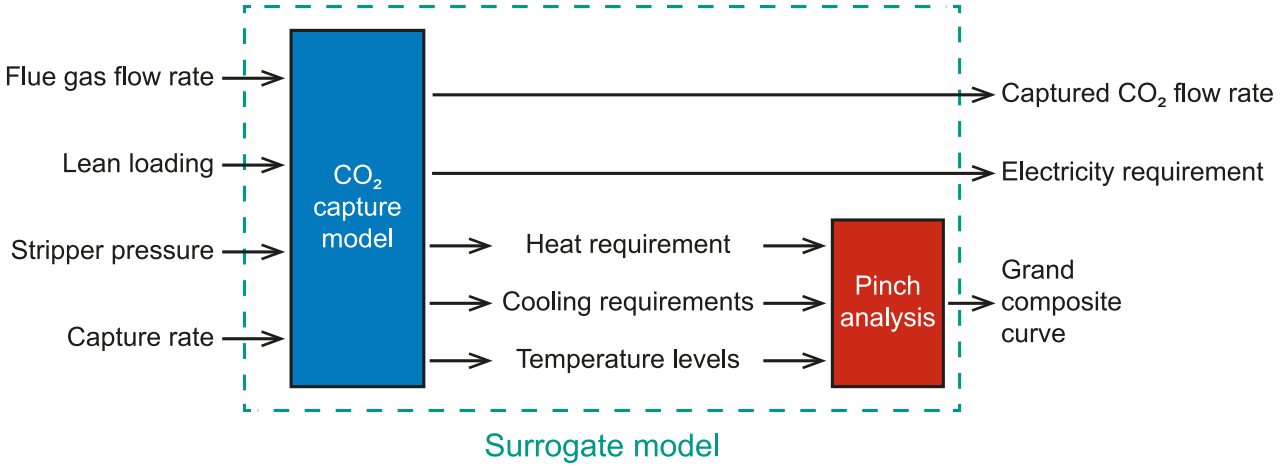

Figure 2. *Inputs and outputs of the model. In total, four inputs are used to build surrogate models for fourteen outputs. Outputs pertaining to thermal energy are further processed through a pinch analysis layer to derive the Grand Composite Curve (GCC).*

Outputs are selected based on the requirements of both the system-level optimisation and the heat pump interface: thermal energy demand, cooling duties, corresponding temperature levels, captured CO_2 flow rate and electricity requirements. In the modelled capture unit, five waste heat sources are available: the condenser at the top of the stripper (stripper overhead condenser, SOC), intercoolers in the CO_2 compression train, the lean solvent cooler before the absorber, the direct contact cooler to condition the inlet flue gas, and the washing section at the absorber outlet. Pinch analysis is implemented as a second modelling layer to transform the relevant thermal outputs into a Grand Composite Curve (GCC).

2.2. Sampling

A range of variation is defined for each input variable. These ranges define the sampling domain, which corresponds to the validity domain of the resulting surrogate model. Bounds are selected to maximise the operational window, consistently with the objective of providing flexibility to the system-level optimiser.

Ranges are reported in Table 1. For all four input variables, lower bounds are selected to minimise convergence issues in Aspen Plus. Indeed, significant deviations from the nominal conditions lead to convergence issues, primarily due to hydraulic and flash calculation failures. The upper bound for flue gas flow rate is chosen as the nominal flow rate. It corresponds to the flue gas emitted during full-power operation of the biomass boiler in the case study. Although lean loading could theoretically reach high values, such operating conditions are unlikely in practice and are associated with convergence issues. The upper bound is therefore selected to minimise such numerical instability. Thermal degradation of the solvent is not included in the model. However, neglecting solvent degradation could compromise the credibility of optimal operating conditions. Stripper pressure is therefore limited to 300 kPa, as it directly influences the reboiler temperature (Figure 1). Finally, while the capture rate is typically set to 90%, recent studies have shown that aiming for higher capture rates is viable [9,10]. The corresponding upper bound is therefore set to 99%.

Table 1. *Input variable ranges.*

Input variable	Lower bound	Upper bound
Flue gas flow rate (*t/h*)	4	44
Lean loading (mol_{CO_2}/mol_{MEA})	0.15	0.35
Stripper pressure (*kPa*)	60	300
Capture rate ($kg_{CO_2,capt}/kg_{CO_2,inlet}$)	0.20	0.99

A total of 1000 samples are generated between the defined ranges using Latin Hypercube Sampling (LHS). LHS ensures a good coverage of the sampling domain. These samples are used as inputs to the Aspen Plus model to evaluate the corresponding output variables.

2.3. Data generation

During simulation, the Aspen Plus model is sensitive to the distance between the target operating point and the previously converged solution. Convergence failures are frequent when operating far from the previous simulation.

A common strategy to simulate operating points far from nominal conditions is to break down the transition into incremental steps and progressively approach the target value. However, because of their multivariate nature, input samples cannot be ordered along a single input dimension.

Instead, a two-step refinement strategy is proposed to improve convergence robustness:

1. Following the approach proposed by Alie et al. [11], the flowsheet is split into several sub-flowsheets, each representing a sub-process of the overall capture system. In total, three flowsheets are solved sequentially: 1) flue gas conditioning and absorber, 2) solvent loop, stripper and CO_2 compression train, and 3) full flowsheet. Unlike Alie et al. [11], the absorber and stripper sub-flowsheets are not iteratively solved to full convergence. Instead, they are individually converged to provide initial guesses for the full flowsheet. If any of the intermediate flowsheets fails to converge, the procedure is interrupted and the input sample is discarded. Each discarded sample reduces the quality of the sampling coverage, so a high convergence success rate is desired.
2. Heuristic rules are applied to several variables to generate initial guesses. For example, temperature estimates are provided to the stripper based on the water saturation temperature at the current stripper pressure. In addition, sensitivity studies are performed to establish multivariate relationships between selected variables and the model inputs, which are then used for initialisation.

With the proposed refinement strategy, a convergence success rate of 96.4% is achieved. To identify potential trends in the remaining convergence failures, histograms of failure counts are presented in Figure 3.

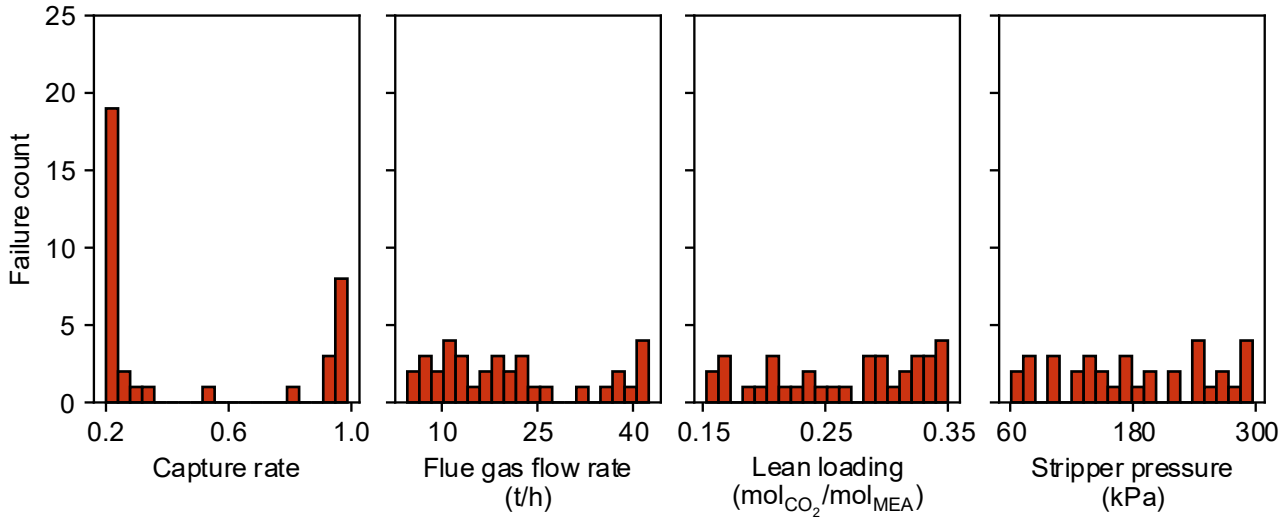

Figure 3. *Out of the 1000 samples, 36 simulations failed, despite the refinement strategy. Each subplot shows the distribution of these 36 failures across the range of each input variable. Most failures occur at extremum values for the capture rate. Low flue gas flow rates and high lean loadings are secondary causes.*

Most convergence failures happen at the extrema of the capture rate range, with sharp concentrations in the distribution. Stripper pressure appears to have limited influence on convergence failures, while low flue gas flow rates and high lean loadings increase the likelihood of failure.

Since failed simulations are discarded, the surrogate model accuracy is expected to decrease near these extrema. Alternatively, the sampling bounds could be further restricted. However, they are retained here, as sufficient valid samples remain in their vicinity due to the high convergence success rate.

2.4. Model training

The remaining 964 data points are randomly split between a training dataset (80%) and a test dataset (20%), used for model training and validation, respectively.

For each output variable (Section 2.1), a surrogate model is constructed as a fourth-degree polynomial (including interaction terms), fitted using multivariate linear regression. The high polynomial degree is justified by low coefficients of determination ($R^2 < 0.95$) at lower degrees. To reduce model complexity, the surrogate structures are inferred from expected physical relationships between inputs and outputs, such that only physically relevant inputs are included in each model. This approach reduces model dimensionality while preserving physical interpretability. For example, the surrogate model for the reboiler heat duty ($\dot{Q}_{th}$) is not constructed as a fourth-order polynomial of all four inputs. Instead, it is reformulated as:

$$\dot{Q}_{th} = \dot{m}_{CO_2} \cdot SRD = \dot{m}_{fg} \cdot y_{CO_2} \cdot \eta \cdot SRD, \qquad (1)$$

where $\dot{m}_{CO_2}$ is the captured CO_2 mass flow rate (kg/s), equal to the product of the flue gas flow rate ($\dot{m}_{fg}$, in kg/s), the CO_2 concentration in the flue gas (y_{CO_2}, in wt.%), and the capture rate (η). The specific reboiler heat duty (SRD, in $MJ_{th}/kgCO_2$) is then modelled as a fourth-order polynomial, using only three inputs ($P_{stripper}, \alpha_{lean}, \eta$). Another example is the cooling duty of the direct contact cooler, which only depends on the flue gas flow rate.

In total, fourteen surrogate models are developed and combined into a single, grey-box model, as illustrated in Figure 2.

2.5. Model validation

The test dataset is used to validate the surrogate models. For each output, the coefficient of determination (R^2) is computed to compare the test dataset values with the corresponding predictions from the surrogate models. For all outputs, high coefficients of determination are obtained ($R^2 > 0.98$). This indicates that the surrogate models accurately capture the input-output relationships over the sampled domain. The risk of overfitting is therefore limited, as the models generalise well to an independent validation dataset.

As an additional validation step, Grand Composite Curves (GCCs) derived from the original data and from model predictions are compared. One such example is depicted in Figure 4. The predicted GCC reproduces the features of the original curve, with noticeable deviations in the 50°C-100°C (shifted) temperature range. This discrepancy corresponds to inaccurate modelling of the partial condensation (i.e. condensation of water in a water-CO_2 mixture) in the stripper overhead condenser (SOC). In this region, the concavity of the T-Q segment is not captured, as the surrogate predicts a linear behaviour. This limitation arises because the fourth-order polynomials defined in the previous section do not directly predict the shape of T-Q segments, but only their boundary points. One possible improvement would be to discretise the corresponding heat transfer, thereby approximating the concave segment with multiple linear segments, at the expense of an increased number of output variables.

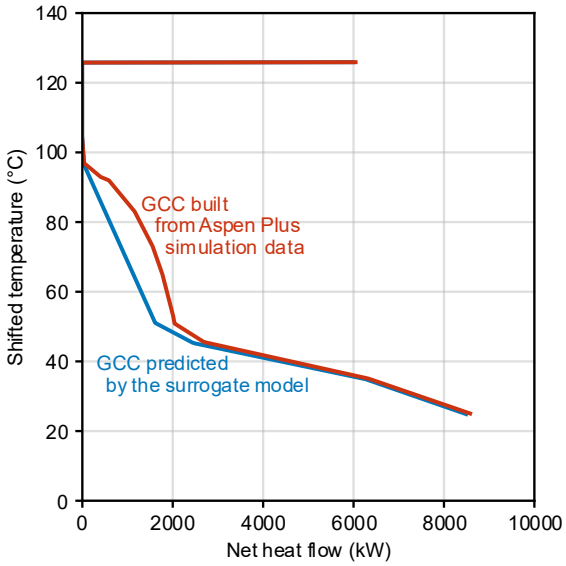

Figure 4. *Grand Composite Curves derived from original data (red) and from model predictions (blue). The main loss of information occurs below the pinch point, where the stripper overhead condenser T-Q curve is linearised. The recoverable waste heat in the corresponding temperature intervals is therefore underestimated.*

2.6. Model application

While accurate, the surrogate model is highly nonlinear, reflecting the underlying physical behaviour of the capture unit. However, most energy system optimisation problems are preferentially defined as linear programming (LP) or mixed-integer linear programming (MILP) problems.

To ensure compatibility with such approaches, the surrogate model would need to be reformulated as a set of piecewise linear (PWL) functions, leading to a MILP formulation. This extension is kept for future works.

In the present work, the polynomial model is retained to provide insights into the integration of the CO_2 capture unit with a high-temperature heat pump, and therefore simplify the future formulation of the MILP problem.

3. Optimal heat pump placement

This section investigates the optimal integration of a high-temperature heat pump within the CO_2 capture process. Using the results from the surrogate model, a pre-screening of the potential integration configurations is performed.

To interface the capture unit with the high-temperature heat pump, the heat pump heat exchangers must be placed within the capture system. The evaporator must draw heat from streams that contribute to the bottom half of the GCC (cold region), while the condenser must supply heat above the pinch point (hot region). Since the reboiler is the sole thermal energy consumer, the heat pump condenser is placed there.

The heat pump evaporator can be placed at one of the cooling heat exchangers (5 opportunities, see Section 2.1) or in a secondary cooling loop that combines several or all of them. Numerous configurations are therefore possible.

The optimal configuration can only be determined by integrating these configurations into the system-level optimisation and letting the optimiser converge towards the cost optimum. In practice, this requires adding an integer variable for each potential configuration and letting the optimiser select configurations from the pool. This introduces a significant amount of optimisation variables and increases significantly the computational complexity of the optimisation problem.

To limit this complexity (i.e. reduce the number of optimisation variables), the polynomial surrogate model is used to study the likelihood of an optimal configuration and therefore reduce the number of configurations to consider.

While cost optimisation is not feasible at this stage, the preliminary screening is still feasible based on operational expenditures (OPEX). In this work, instead of dealing with OPEX and the required cost assumptions, energy usage is studied. This neglects other components of OPEX as well as capital expenditures (CAPEX), under the assumption that both do not vary significantly across configurations. In other words, integration configurations with optimal energy usage are expected to be promising candidates.

In the context of a multi-vector energy system, a common comparison basis is required to integrate the different energy carriers into a single metric. Exergy is selected for that purpose. Since it accounts for energy quality, it provides a relevant proxy for operational costs [12].

The total exergy of a combined CO_2 capture-heat pump configuration is defined as the sum of:

- the exergy associated with heat supply ($\dot{X}_{heating}$),
- the exergy associated with cooling duties ($\dot{X}_{cooling}$),
- the exergy associated with CO_2 compression ($\dot{X}_{compression}$, equal to the work of compression),
- and the exergy associated with heat pumping ($\dot{X}_{hp}$).

Indeed, heat that is neither supplied (above the pinch point) nor consumed (below the pinch point) by the heat pump must still be dealt with by conventional means. The Carnot factor $\left(1-\frac{T_0}{T}\right)$ is used to calculate the corresponding exergies of heating and cooling from the heat transfers occurring at a temperature T (T_0 is the environment temperature, taken as 298.15 K). In the case study, heat is assumed to be available as medium pressure steam (225°C) and cooling occurs at 20°C.

The evaporator placement problem is therefore formulated as an exergy minimisation problem:

$$\min_{T_{evap},\ \dot{Q}_{evap}} \dot{X}_{total} = \dot{X}_{heating} + \dot{X}_{cooling} + \dot{X}_{compression} + \dot{X}_{hp}, \qquad (2)$$

where T_{evap} is the temperature at which the evaporator draws the heat $\dot{Q}_{evap}$.

From a GCC generated by the surrogate model, an optimisation routine is implemented to find the pair $(T_{evap}, \dot{Q}_{evap})$ that minimises the objective function (Eq. 2). The GCC imposes a constraint on heat availability, since waste heat availability at a given temperature level T^* is bounded such that $\dot{Q}_{evap}(T^*) \leq \dot{Q}_{GCC}(T^*)$.

Using Latin Hypercube Sampling (LHS), 5000 samples are generated between the bounds defined in Section 2.2. For each sample, the corresponding Grand Composite Curve (GCC) is predicted by the CO_2 capture surrogate model (Section 2.4). The heat pump condenser is placed at the temperature level of the reboiler (which depends on the input stripper pressure), and the heat pump evaporator is placed at one or several heat exchangers following the exergy minimisation problem formulated before. In this process, the heat pump is modelled using a Carnot-based approach but a second-law efficiency of 50% is accounted for to reflect the current reported performance of high-temperature heat pumps [5].

The resulting heat pump integration configurations are illustrated in Figure 5, in which the evaporator temperature represents the heat pump placement. Two dominant integration scenarios emerge.

In most cases, a heat pump is placed at an evaporator temperature between 60°C and 80°C. In that configuration, the heat pump only draws heat from two sources: the stripper overhead condenser (SOC) and

the intercoolers of the CO_2 compression train. Due to limited heat availability at these sources, the heat pump capacity remains low and can only provide a fraction of the total heat supply, meaning that a conventional thermal energy supply is still required. In other words, steam withdrawal from the CHP plant is more interesting than increasing the temperature lift of the heat pump in that scenario.

The second most dominant integration exhibits a lower evaporator temperature (around 40°C). In that scenario, most waste heat sources are aggregated to supply the heat pump evaporator. At lower temperatures, cumulative waste heat availability is higher, and the heat pump is able to supply the entire thermal energy requirement of the capture process (the contribution to heat supply reaches 100%).

These two configurations are complemented by some in-between cases, with fewer occurrences. In very few cases, only the SOC is used, and the heat pump contributes to the total heat supply by a very low amount. In other cases, three or four sources are used.

Instead of explicitly modelling a larger number of configurations in the system-level optimisation, it is possible to limit the pool of potential integrations to less than five configurations, or even down to two configurations. Instead of many integer values, much less optimisation variables are needed. The fraction of available waste heat that is indeed consumed is one of them. This significantly reduces the complexity of the optimisation model.

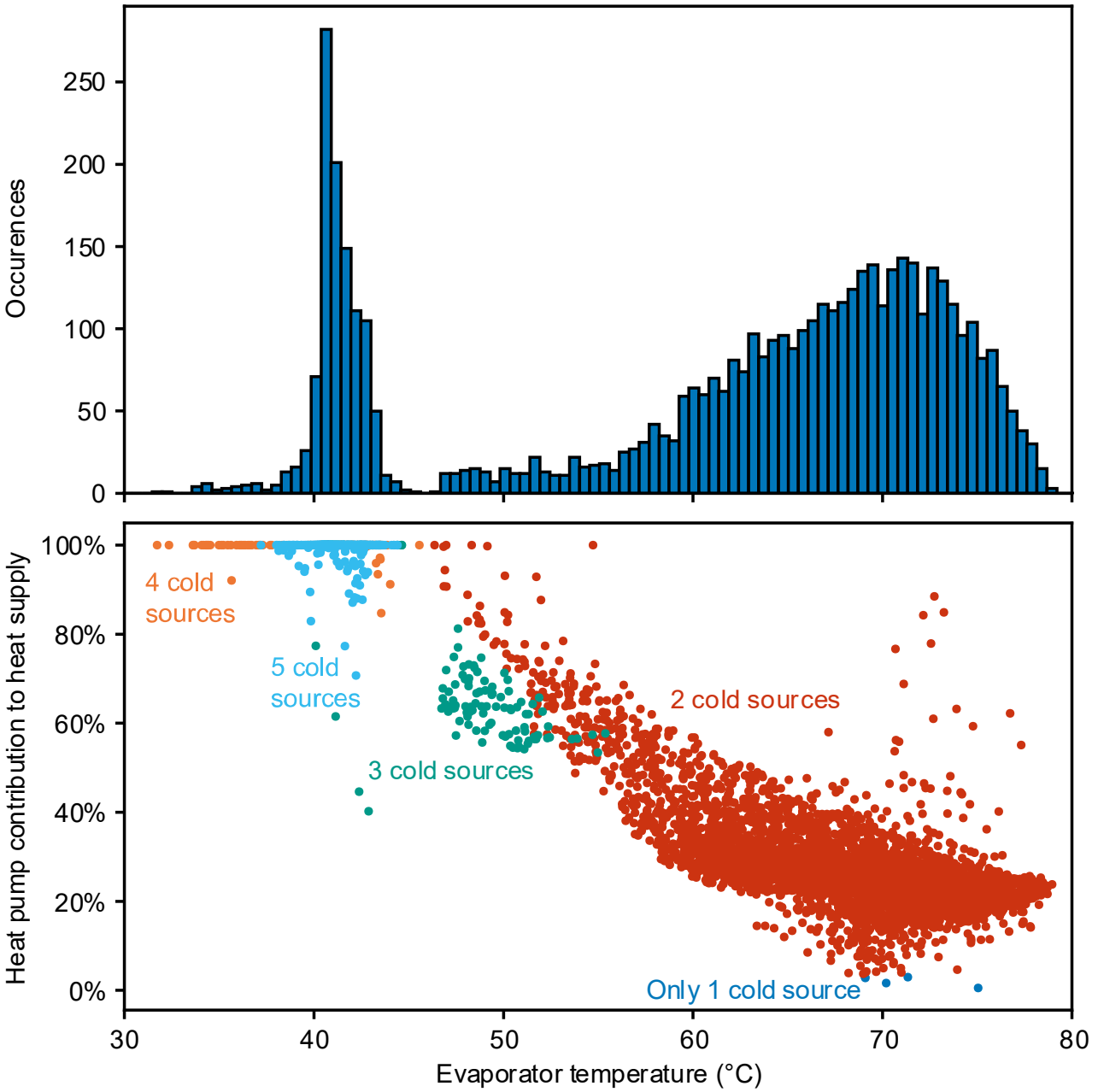

Figure 5. *Resulting optimal heat pump placements built from surrogate model results. Each point represents the operation of the capture system with a different set of inputs and the corresponding optimal integration of a heat pump by exergy minimisation.*

To identify the conditions under which the optimal integration shifts between configurations, a pairwise projection plot is presented in Figure 5. It represents the 4D sampling space projected onto all possible pairs of input variables. Each point corresponds to one of the 5000 samples. The colour scale indicates the contribution of the heat pump to the total heat supply. As shown in Figure 4, higher heat pump contribution correlate with lower evaporator temperatures, and therefore with the involvement of additional waste heat sources. The two dominant configurations identified earlier can therefore be associated with regions of low (blue) and high (yellow) heat pump contribution, respectively.

Stripper pressure (bottom row in Figure 6) is the primary parameter that governs the selection between configurations. Physically, decreasing stripper pressure reduces the reboiler temperature (Figure 1), thereby reducing the required heat supply temperature. As a result, the required temperature lift decreases, or equivalently, a larger amount of waste heat becomes available for a given temperature lift. Heat supply via heat pumping therefore becomes less exergy-intensive, making it more favourable than conventional steam supply.

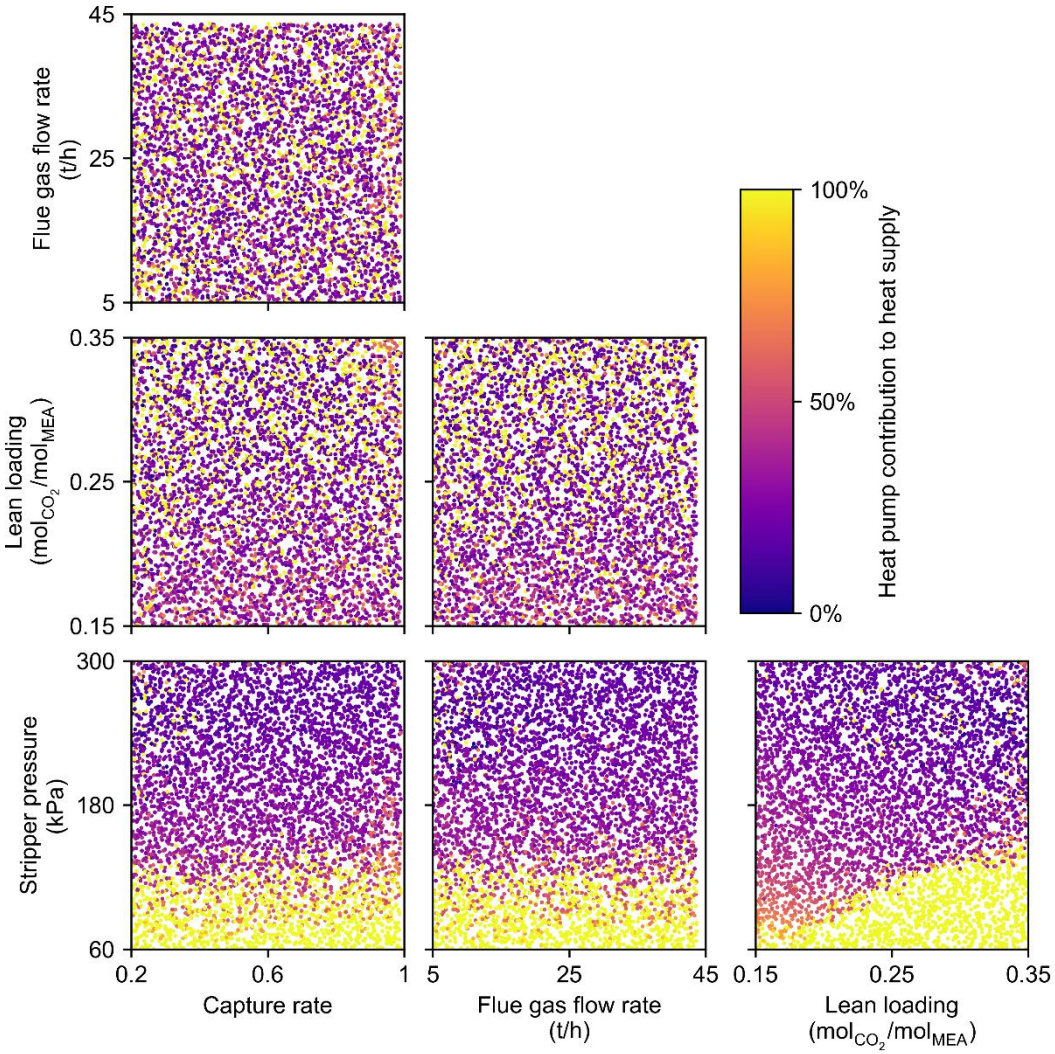

Figure 6. *Pairwise projection plot of 5000 heat pump placements simulated from surrogate model results. The colour scale indicates the relative heat pump contribution to heat supply.*

At low stripper pressures, lean loading also affects the optimal heat pump placement, with higher lean loadings leading to configurations with greater heat pump contributions. This behaviour can be explained by two underlying mechanisms:

- As lean loading increases, the solvent absorption capacity decreases, requiring an increase in the solvent flow rate to maintain the target capture rate. Consequently, the cooling duty of the lean solvent cooler increases. This modifies the GCC by introducing a flatter segment, leading to increased recoverable waste heat and therefore higher heat pump contributions for a given temperature lift.
- In addition, there exists an optimal lean loading that minimises the reboiler heat duty. As stripper pressure decreases, this optimum shifts towards higher lean loadings (Figure 7). For low lean loadings, the specific reboiler heat duty (SRD) increases sharply as stripper pressure decreases, due to the increasing distance

from the optimal operating point. As a result, the overall heat demand increases, reducing the relative contribution of the heat pump to the total heat supply.

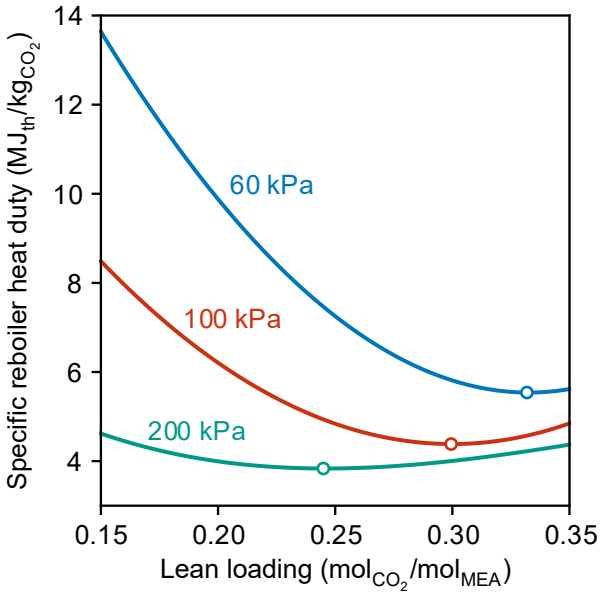

Figure 7. *Predicted specific reboiler heat duty (SRD) as a function of lean loading for different stripper pressures. The minimum (highlighted on each curve) shifts towards higher lean loadings as stripper pressure decreases. At low lean loadings, the SRD increases significantly with decreasing pressure due to the growing distance from the optimal operating point.*

While this analysis identifies promising configurations for future system-level optimisation, it does not determine the global optimal operating point. Indeed, it is not guaranteed that a higher heat pump contribution leads to lower overall system costs. Nevertheless, the results highlight how process flexibility can reshape heat recovery opportunities. When integrated into a broader energy system, these interactions can lead to distinct operating regimes that may be exploited by the optimiser, especially under varying market conditions and energy availability.

Finally, these results indicate that full electrification of the capture unit by means of a high-temperature heat pump is feasible, but requires operation under specific conditions (low stripper pressure and high lean loading) associated with higher total energy consumption. For such configurations to be economically viable, electricity must be significantly more cost-competitive than conventional thermal energy sources. With the expected large-scale deployment of renewable electricity, such conditions may become increasingly plausible.

4. Conclusion and perspectives

Integrating CO_2 capture into multi-vector energy systems requires computationally efficient models capable of capturing nonlinear process behaviour. In this work, a physics-informed polynomial surrogate model of an amine-based CO_2 capture unit was developed from a high-fidelity Aspen Plus model in the context of a biomass-fired CHP case study.

Model inputs were selected to introduce operational flexibility by enabling part-load and off-optimum operation. A convergence-assistance algorithm was developed to ensure robust data generation across the sampling domain, leading to a high convergence success rate (96.4%).

The surrogate model was specifically designed to interface with an external high-temperature heat pump as a means of electrification to take advantage of the multi-vector nature of the energy system. Heat integration was performed using pinch analysis to generate Grand Composite Curves (GCCs), mapping both heat demand and recoverable waste heat.

The model structure was based on physical relationships between input and output variables. This approach enabled accurate prediction of energy requirements while preserving interpretability and reducing model complexity.

Exergy minimisation was conducted to identify the optimal heat pump placement in the capture unit for various operating points. The analysis reveals that two dominant heat pump integration configurations emerge: a partial integration relying on high-temperature waste heat sources, and a full electrification scenario exploiting low-temperature heat across the entire process. The transition between these configurations is primarily governed by stripper pressure, which controls the reboiler temperature and thus the required temperature lift, and secondarily by lean loading, which impacts both reboiler heat duty and solvent flow rate.

These results highlight that operating the capture unit at its standalone energy optimum does not necessarily lead to optimal system-level integration. Instead, off-optimum operation can lead to additional synergies, particularly with heat pump integration in this context. Full electrification of the capture process is technically feasible but appears to be preferable under conditions that favour low temperature lifts and low-cost electricity.

More broadly, this work demonstrates that surrogate models can serve not only for computationally efficient predictions, but also as tools for exploring thermodynamic integration configurations in complex energy systems. The combination of surrogate modelling and exergy-based analysis also provides a framework for pre-screening process configurations prior to system-level optimisation.

Future work should focus on three main directions. First, integration into system-level optimisation requires reformulation of the surrogate model as piecewise linear (PWL) functions and a corresponding mixed-integer linear programming (MILP) framework. Second, process modelling can be refined by improving the representation of the partial condenser and by choosing rate-based process unit models to better capture off-optimum operation. Third, broader integration opportunities should be explored, including extending pinch analysis to other system components and investigating alternative heat pump configurations such as open-loop systems (e.g. lean vapour compression).

Ultimately, the results highlight the importance of operational flexibility in enabling the integration of CO_2 capture within energy systems. As renewable electricity becomes increasingly available, the coupling between CO_2 capture and electrification technologies is expected to play a key role in achieving cost-effective negative emissions in biomass-fired multi-vector energy systems.

Acknowledgements

This publication was supported by the Walloon Region through a FRIA grant.

Nomenclature

Letter symbols

$\dot{Q}$ heat flow, W

$\dot{m}$ mass flow rate, kg/s

y mass concentration, wt.%

P pressure, Pa

$\dot{X}$ exergy flow, W

T temperature, °C or K

Greek symbols

η capture rate

α lean loading, $\mathrm{mol}_{\mathrm{CO_2}}/\mathrm{mol}_{\mathrm{MEA}}$

Subscripts and superscripts

th thermal

CO_2 captured CO_2

fg flue gas

hp heat pumping

0 reference state

$evap$ evaporator

GCC grand composite curve

References

[1] Bui M, S. Adjiman C, Bardow A, J. Anthony E, Boston A, Brown S, et al. Carbon capture and storage (CCS): the way forward. Energy & Environmental Science 2018;11:1062–176. https://doi.org/10.1039/C7EE02342A.

[2] Fluxys Belgium SA. Carbon Specification Proposal. 2022.

[3] Jiang J, Hu B, Wang RZ, Deng N, Cao F, Wang C-C. A review and perspective on industry high-temperature heat pumps. Renewable and Sustainable Energy Reviews 2022;161:112106. https://doi.org/10.1016/j.rser.2022.112106.

[4] Arpagaus C, Bless F, Uhlmann M, Schiffmann J, Bertsch SS. High temperature heat pumps: Market overview, state of the art, research status, refrigerants, and application potentials. Energy 2018;152:985–1010. https://doi.org/10.1016/j.energy.2018.03.166.

[5] Annex 58 (IEA Heat Pumping Technologies). High-Temperature Heat Pumps – Task 1: Technologies. 2023.

[6] Kemp IC. Pinch analysis for energy and carbon footprint reduction: user guide to process integration for the efficient use of energy. Third edition. Kidlington, Oxford: Butterworth-Heinemann; 2020.

[7] Freguia S, Rochelle GT. Modeling of CO2 capture by aqueous monoethanolamine. AIChE Journal 2003;49:1676–86. https://doi.org/10.1002/aic.690490708.

[8] Abu-Zahra MRM, Schneiders LHJ, Niederer JPM, Feron PHM, Versteeg GF. CO2 capture from power plants: Part I. A parametric study of the technical performance based on monoethanolamine. International Journal of Greenhouse Gas Control 2007;1:37–46. https://doi.org/10.1016/S1750-5836(06)00007-7.

[9] Brandl P, Bui M, Hallett JP, Mac Dowell N. Beyond 90% capture: Possible, but at what cost? International Journal of Greenhouse Gas Control 2021;105:103239. https://doi.org/10.1016/j.ijggc.2020.103239.

[10] Feron P, Cousins A, Jiang K, Zhai R, Shwe Hla S, Thiruvenkatachari R, et al. Towards Zero Emissions from Fossil Fuel Power Stations. International Journal of Greenhouse Gas Control 2019;87:188–202. https://doi.org/10.1016/j.ijggc.2019.05.018.

[11] Alie C, Backham L, Croiset E, Douglas PL. Simulation of CO2 capture using MEA scrubbing: a flowsheet decomposition method. Energy Conversion and Management 2005;46:475–87. https://doi.org/10.1016/j.enconman.2004.03.003.

[12] Deng L, Adams II TA, Gundersen T. Exergy Tables: A Comprehensive Set of Exergy Values to Streamline Energy Efficiency Analysis. First edition. New York, N.Y: McGraw Hill LLC; 2024.